

Multi-Conjugate Adaptive Optics with two Deformable Mirrors - Requirements and Performance

Thomas Berkefeld (berke@kis.uni-freiburg.de)
Kiepenheuer-Institut für Sonnenphysik, Freiburg, Germany

Andreas Glindemann (aglindem@eso.org)
European Southern Observatory, Garching, Germany

Stefan Hippler (hippler@mpia-hd.mpg.de)
Max-Planck-Institut für Astronomie, Heidelberg, Germany

Abstract. In order to increase the corrected field of view of an adaptive optics (AO) system, several deformable mirrors (DM) have to be placed in the conjugate planes of the dominant turbulent layers (multi-conjugate adaptive optics, MCAO (Beckers, 1988)). The performance of MCAO systems depends on the quality of the wavefront sensing of the individual layers and on the number of corrected modes in each individual layer as in single layer AO systems. In addition, the increase in corrected field of view depends on the number of guide stars providing information about the turbulence over a sufficiently large area in each turbulent layer. In this paper, we investigate these points and provide formulae for calculating the increased field of view with a new approach using the spatial correlation functions of the applied polynomials (e.g. Zernike). We also present a new scheme of measuring the individual wavefront distortion of each of the dominant layers with a Shack-Hartmann-Curvature Sensor using gradient information as well as scintillation. An example for the performance of a two layer MCAO system is given for the 3.5-m telescope of the Calar Alto Observatory, Spain, using a measured C_n^2 -profile. The corrected field of view in K-band ($2.2\mu\text{m}$) can be as large as 3 arcmin with a Strehl ratio above 60%.

Keywords: adaptive optics, multi-conjugate adaptive optics, laser guide stars, turbulent layers

Abbreviations: AO – Adaptive Optics; MCAO – Multi-Conjugate Adaptive Optics; DM – Deformable Mirror; LGS – Laser Guide Star; NGS – Natural Guide Star; GS – Guide Star; SH – Shack-Hartmann; SHC – Shack-Hartmann-Curvature; NIR – Near-Infrared

1. Introduction

While AO systems increase the angular resolution of ground based telescopes by a factor of 5–20, their most severe disadvantage is the very small corrected field of view which is typically of the order of $30''$ in K-band ($2.2\mu\text{m}$) and only a few arc seconds in the visible. MCAO systems with several DMs in the conjugate planes of the dominant turbulent layers as proposed by Beckers (1988) have two important advantages over conventional AO systems:

- The corrected field of view is increased considerably by correcting the dominant turbulent layers instead of correcting the integrated wavefront aberrations even if the turbulence is not located in distinct layers.



- Focal anisoplanatism which is a severe limitation for Laser Guide Star (LGS) AO systems can be almost completely eliminated by using multiple LGSs (see Sect. 2.2).

The optimal position of the DMs is determined by the C_n^2 -profile and by the system characteristics e.g. the size of the corrected field of view and the number of corrected modes. Usually the angular anisoplanatism of AO systems is calculated according to the $(\theta/\theta_0)^{(5/3)}$ -law (Tyson, 1991). For real systems however the corrected field of view is larger than given by this formula. Therefore a more realistic calculation is needed, both for estimating the performance of AO and MCAO systems, i.e. the corrected FOV, and for obtaining the optimal position of the DMs in MCAO systems. This is done in section 2, where we derive an equation for calculating the anisoplanatism both for AO and MCAO systems using correlation functions of the applied Zernike polynomials. The anisoplanatism depends on the C_n^2 -profile, the number of corrected modes of each layer, the number and position of the DMs and the angle between science object and central guide star. Using various MCAO geometries, we apply these formulae to calculate the Strehl ratios for a 3.5-m telescope and for a turbulence profile measured by Klückers (Klückers et al., 1998) at the Calar Alto Observatory.

The second important issue of MCAO is the problem of wavefront sensing distinguishing the turbulent layers. Section 3.1 gives a short introduction to scintillation and describes the principle of separating the wavefront distortions of two turbulent layers with a Shack-Hartmann (SH) sensor (Ribak, 1996; Schwartz et al., 1994) or a Shack-Hartmann-Curvature (SHC) sensor (Glindemann and Berkefeld, 1996), both using intensity fluctuations. By varying the effective altitude of the wavefront sensor(s) the SNR of the scintillation signal can be optimized. It will be shown in Section 3.3 that a SHC sensor allows for much fainter guide stars than a SH sensor. Furthermore, the SH sensor delivers only one scintillation signal, therefore wavefront modes with zero-Laplacian cannot be properly measured. With a SHC sensor, however, the second scintillation signal can reduce the error induced by these modes.

A good introduction for the concept of MCAO can be found in Beckers (1988), more recent investigations of its applicability and performance were presented by Johnston and Welsh (1994).

Unless mentioned otherwise, the wavelength used corresponds to the K-band ($2.2\mu\text{m}$).

2. The wavefront error σ_θ^2 of angular anisoplanatism

The wavefront error due to angular anisoplanatism is denoted by σ_θ^2 . It is caused by slightly different turbulence patterns in the light paths of two stars. σ_θ^2 can be expressed as

$$\sigma_\theta^2 = \left(\frac{\theta}{\theta_0} \right)^{5/3}, \quad (1)$$

where θ denotes the angular separation of the two stars. θ_0 is the *isoplanatic angle* that is defined such that $\sigma_\theta^2 < 1$ for objects lying inside the isoplanatic patch (Tyson, 1991). θ_0 has to be defined in such a way that the number of corrected modes is taken into account: A simple tip/tilt system has a much larger isoplanatic angle than higher order AO-systems. For the special cases of a tip/tilt system and certain higher order systems Sasiela and Shelton (1993) and Chassat (1989) already derived expressions.

2.1. ANGULAR ANISOPLANATISM OF AO-SYSTEMS

The following approach of calculating σ_θ^2 is based on the cross-correlation function $C_{x,y}$ of two tip/tilt measurements at b and at b' and includes the general dependence of the isoplanatic patch on the degree of correction.

Measurements of correlation functions yield important information about the parameters of AO systems: The temporal autocorrelation of tilt measurements determines the necessary bandwidth of the control loop and the correlation of tilt measurements of different stars (spatial correlation) allows us to calculate of the isoplanatic angle.

The differential jitter of two beams caused by anisoplanatism is (Valley and Wandzura, 1979)

$$\langle (b - b')^2 \rangle_{x,y} = 2[1 - C_{x,y}] \cdot \langle b^2 \rangle, \quad (2)$$

where x- and y- directions correspond to the directions parallel and perpendicular to the line of sight between the two stars. $\langle b^2 \rangle$ represents the one dimensional variance of the tilt. The variance of the differential image motion can be written as

$$\begin{aligned} (\Delta\theta)^2 &= \langle (b - b')^2 \rangle_x + \langle (b - b')^2 \rangle_y \\ &= ((1 - C_x(\theta)) + (1 - C_y(\theta))) \cdot 2\langle b^2 \rangle, \end{aligned} \quad (3)$$

where $2\langle b^2 \rangle$ is the two-axis variance of the position angle b . The variance $\langle b^2 \rangle$ of the position angle is related linearly to the wavefront error due to G-tilt¹. In a very similar fashion, one can write the wavefront error $\sigma_{\theta,tt}^2$ of the

¹ The wavefront error related to the motion of the image centroid is often called G-tilt since it is equivalent to the average gradient of the wavefront over the telescope aperture.

Zernike tilt - the first mode (apart from piston) of the Zernike decomposition
- due to differential image jitter as

$$\begin{aligned}\sigma_{\theta,tt}^2 &= ((1 - C_{tt,x}(\theta)) + (1 - C_{tt,y}(\theta))) \cdot 2 \cdot 0.448 \left(\frac{D}{r_0}\right)^{5/3} \\ &= 2 \cdot \left(\frac{D}{r_0}\right)^{5/3} \cdot 0.448 \cdot (2 - C_{tt,x}(\theta) - C_{tt,y}(\theta)).\end{aligned}\quad (4)$$

$0.448(D/r_0)^{5/3}$ is the wavefront variance of the single axis tilt as given by Noll (1976). As soon as the correlation functions $C_{tt,x,y}(\theta)$ have a value smaller than 0.5 the resulting tip-tilt correction with an on axis guide star deteriorates the image quality since the wavefront error becomes larger than $0.448(D/r_0)^{5/3}$, *i.e.* larger than the uncorrected value. Eventually, for zero correlation the variance is twice as large as without correction.

The anisoplanatism of higher order wavefront modes can be deduced in a similar fashion (see Berkefeld (1998), corrected for minor inaccuracies in the deduction). Then, the wavefront error $\sigma_{\theta,N}^2$ as a function of the correlation of N corrected Zernike modes can be written as

$$\sigma_{\theta,N}^2 = 2 \left(\frac{D}{r_0}\right)^{5/3} \cdot \sum_{j=1}^N (\sigma_{\text{fit},j-1}^2 - \sigma_{\text{fit},j}^2)(1 - C_j(\theta)),\quad (5)$$

summing up the different correlations $C_j(\theta)$ of each mode j and the modal variance $\sigma_{\text{fit},j-1}^2 - \sigma_{\text{fit},j}^2$ to the wavefront error. The total wavefront error for a star at a distance θ from the guide star can then be calculated by adding $\sigma_{\theta,N}^2$ to the fitting error $\sigma_{\text{fit},j>N}^2$. Eq. 5 can be used with any set of polynomials if the correlation functions and the modal variances are available. Chassat (1989) presented results for $\sigma_{\theta,N}^2$ for selected Zernike-polynomials.

Table I shows σ_{fit}^2 for Kolmogorov turbulence described by Zernike polynomials as a function of the number j of corrected modes (see Noll (1976)).

For $j > 20$, $\sigma_{\text{fit},j}^2$ can be approximated by

$$\sigma_{\text{fit},j}^2 \approx 0,2944 (j+1)^{-\sqrt{3}/2} (D/r_0)^{5/3}.\quad (6)$$

For an AO system with an LGS at infinity, *i.e.* without the cone effect, and an NGS for tip-tilt the wavefront error $\sigma_{\theta,N,LGS}^2$ becomes

$$\begin{aligned}\sigma_{\theta,N,LGS}^2 &= 2 \cdot \left(\frac{D}{r_0}\right)^{5/3} [0.448 \cdot (2 - C_x(\theta_{NGS}) - C_y(\theta_{NGS})) + \\ &\quad \sum_{j=3}^N (\sigma_{\text{fit},j-1}^2 - \sigma_{\text{fit},j}^2)(1 - C_j(\theta_{LGS}))].\end{aligned}\quad (7)$$

Table I. Wavefront error for Kolmogorov-turbulence described by Zernike polynomials as a function of the number j of corrected modes (Noll (1976)).

$\sigma_{\text{fit},0}^2 = 1.0299(D/r_0)^{5/3}$	$\sigma_{\text{fit},7}^2 = 0.0525(D/r_0)^{5/3}$	$\sigma_{\text{fit},14}^2 = 0.0279(D/r_0)^{5/3}$
$\sigma_{\text{fit},1}^2 = 0.5820(D/r_0)^{5/3}$	$\sigma_{\text{fit},8}^2 = 0.0463(D/r_0)^{5/3}$	$\sigma_{\text{fit},15}^2 = 0.0267(D/r_0)^{5/3}$
$\sigma_{\text{fit},2}^2 = 0.1340(D/r_0)^{5/3}$	$\sigma_{\text{fit},9}^2 = 0.0401(D/r_0)^{5/3}$	$\sigma_{\text{fit},16}^2 = 0.0255(D/r_0)^{5/3}$
$\sigma_{\text{fit},3}^2 = 0.1110(D/r_0)^{5/3}$	$\sigma_{\text{fit},10}^2 = 0.0377(D/r_0)^{5/3}$	$\sigma_{\text{fit},17}^2 = 0.0243(D/r_0)^{5/3}$
$\sigma_{\text{fit},4}^2 = 0.0880(D/r_0)^{5/3}$	$\sigma_{\text{fit},11}^2 = 0.0352(D/r_0)^{5/3}$	$\sigma_{\text{fit},18}^2 = 0.0232(D/r_0)^{5/3}$
$\sigma_{\text{fit},5}^2 = 0.0648(D/r_0)^{5/3}$	$\sigma_{\text{fit},12}^2 = 0.0328(D/r_0)^{5/3}$	$\sigma_{\text{fit},19}^2 = 0.0220(D/r_0)^{5/3}$
$\sigma_{\text{fit},6}^2 = 0.0587(D/r_0)^{5/3}$	$\sigma_{\text{fit},13}^2 = 0.0304(D/r_0)^{5/3}$	

The correlation functions $C_j(\theta)$ of the individual Zernike modes j are

$$C_j(\theta) = \frac{\int c_j(z\theta)C_n^2(z) dz}{\int C_n^2 dz}, \quad (8)$$

where $c_j(z\theta) = c_j(d)$ denotes the correlation caused by a single layer at altitude z (Valley and Wandzura (1979)). Figure 1 shows the correlation for different aberrations as a function of the parameter d/D . Higher order aberrations generally decorrelate faster because they correspond to smaller structures (and thus smaller correlation lengths).

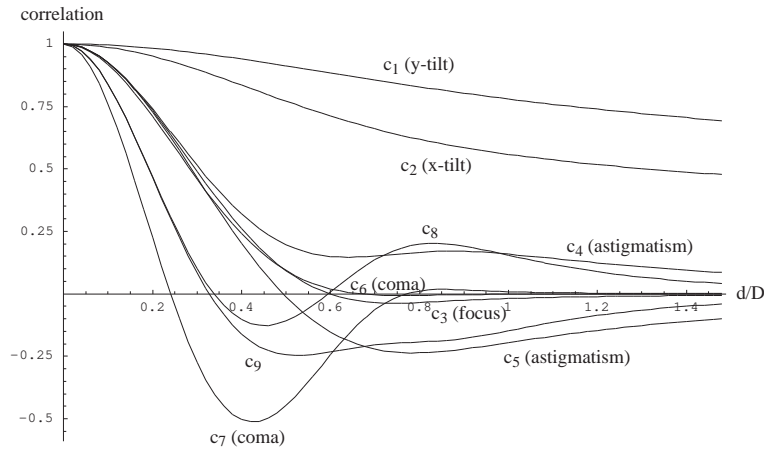


Figure 1. Correlation functions $c_j(d)$ for different Zernike-modes as a function of the light path offset d and the aperture D

The turbulence profile C_n^2 determines the correlation functions $C_j(\theta)$ used in the above equations. If C_n^2 is unknown, higher order correlations can be approximately derived from the measured tip/tilt correlations in pure Kolmogorov turbulence.

Inserting $C_j(\theta)$ into Eq. 5 yields the wavefront variance $\sigma_{\theta,N}^2$ for N corrected modes. The isoplanatic angle θ_0 can then be calculated such that $\sigma_{\theta_0,N}^2 = 1$. Fig. 2 shows the Strehl ratio for the wavefront variance given by $\sigma_{\text{fit}}^2 + \sigma_{\theta,N}^2$ as a function of the number of corrected modes and the angle between science object and guide star. Because of the fast decorrelation of the higher modes, a low order correction can yield higher Strehl ratios at large distances between object and guide star (see Fig. 2).

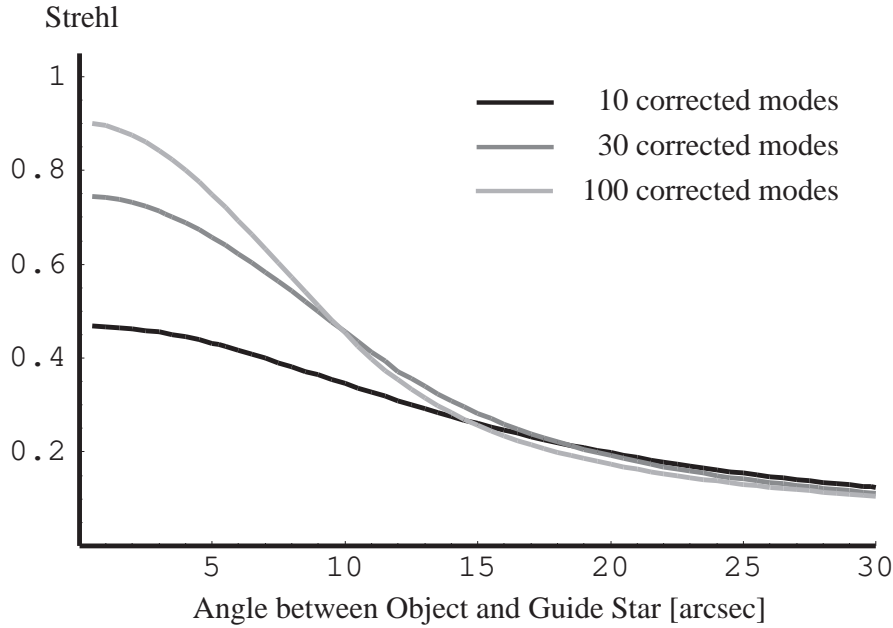


Figure 2. Strehl ratio for the wavefront variance $\sigma_{\text{fit}}^2 + \sigma_{\theta}^2$ as a function of the number of corrected modes and the angle between science object and guide star ($D = 3.5$ m, single turbulent layer at 5000 m, $r_0 = 60$ cm)

2.2. ANGULAR ANISOPLANATISM OF MCAO-SYSTEMS

In the case of an MCAO system with M DMs at conjugated altitudes z_i , the correlation $C_j(\theta)$ becomes

$$C_j(\theta) = \left(\sum_{i=1}^M \int_{(z_{i-1}+z_i)/2}^{(z_i+z_{i+1})/2} c_j(|z_i - z|\theta) C_n^2(z) dz \right) / \int_0^{\infty} C_n^2(z) dz, \quad (9)$$

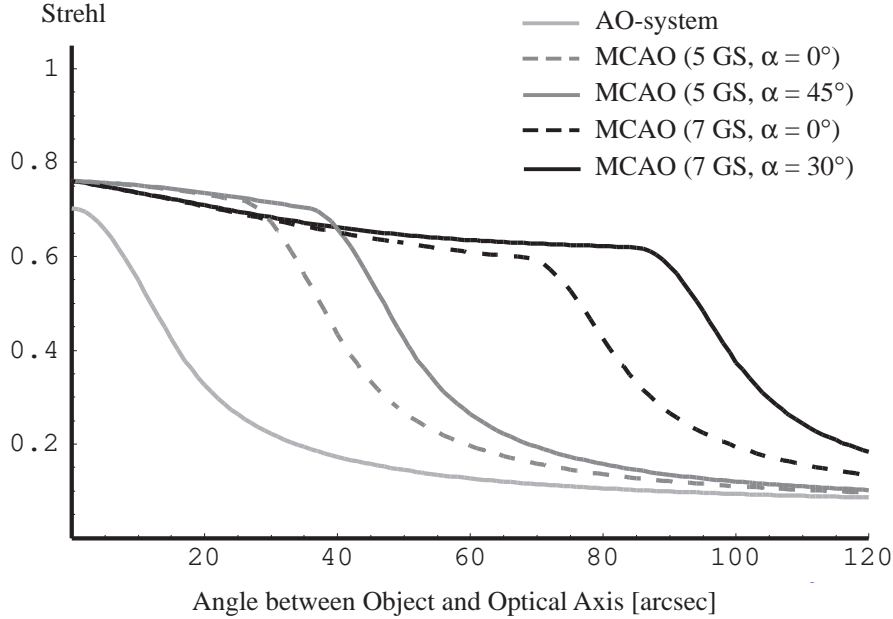


Figure 4. Strehl ratio for the wavefront variance $\sigma_{\text{fit}}^2 + \sigma_{\theta}^2$ as a function of the angle between object and central LGS for a 2 DM MCAO system and LGS geometries shown in Fig. 5 (see section 2.3). For comparison the Strehl ratio is also given for a conventional AO system. The parameters are: telescope aperture $D = 3.5$ m, Calar Alto C_n^2 -profile, K-Band and 37 corrected modes. The Strehl ratio depends both on the azimuth angle α and the distance to the central LGS. The tip/tilt of each LGS is assumed to be known. The superiority of an MCAO system over an AO system, especially when seven LGSs are used, is obvious. The diameter of the corrected field of view can be as large as 3 arcmin. Due to the corrected *cone effect*, the MCAO system shows better performance even at the field center.

2.3. LASER GUIDE STAR GEOMETRY

To measure the wavefront distortion, several guide stars are necessary to cover the field. Since it is unlikely to find natural guide stars at the desired positions, LGSs will be necessary in most cases. Mapping the wavefront distortion over the desired field requires the LGSs to be pointed such that their light cones still overlap at the altitude of the highest turbulent layer (see Fig. 5).

Usually the science object does not coincide with an LGS, so different parts of the wavefront intersect different LGS light cones and are corrected accordingly. Therefore the anisoplanatism depends on the angular distance to different LGSs. In this paper, the fraction of intersection of each LGS is taken as a weighting factor for its contribution to anisoplanatism. This approximation leads to a linear Strehl ratio decrease close to the field center, see Fig. 4 (instead of a more gaussian-like decrease, see Fig. 2). However, it is also possible to achieve an almost flat Strehl ratio over the FOV if the

peak Strehl ratio at the field center is sacrificed for achieving a higher Strehl ratio at the edge of the field. Fig. 4 shows the Strehl ratio as a function of the azimuth angle α and the angular distance between the object and the central LGS. It is obvious that seven LGSs lead to a larger and more evenly covered field of view than five LGSs, although the Strehl ratio drop-off due to residual angular anisoplanatism is slightly higher.

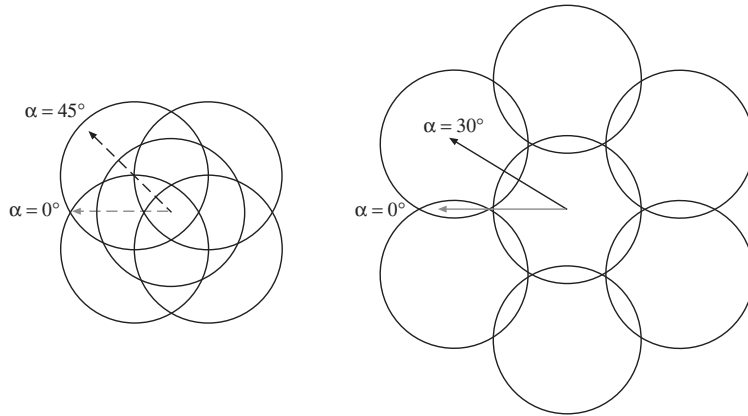


Figure 5. Top view at the highest turbulent layer. Five (left) and seven (right) LGSs have been used for the following calculations. Each circle denotes the illuminated area of the light cone from an LGS in the turbulent layer. If e.g. the Calar Alto turbulence profile is taken the Sodium layer at 90 km and the turbulent layer at 7 km result in a illuminated circle with a diameter of 92% of the aperture of the telescope. These parameters are used throughout this paper. For measuring the wavefront distortion over the desired field of view, the light cones, i.e. the corresponding subapertures of the wavefront sensors have to cover the field of view completely. The field angles used for Fig. 4 (0° , 30° , 45°) are also shown.

The positions of the LGSs correspond to the highest accuracy for wavefront sensing (as in AO-systems, no angular anisoplanatism). At low altitudes, however, the light cones of the LGSs overlap almost completely. The wavefront reconstructions of the low layer are slightly different for the individual LGSs because the extended turbulent layers are reduced to thin layers. Since one has to choose one reconstruction to steer the mirror we used the central LGS, which defines the center of the corrected FOV. The angular anisoplanatism of the other LGS positions is mainly due to this low altitude correction. For high altitudes and little overlap between neighbouring light cones, more degrees of freedom allow a correction close to the optimum, as can be seen in Fig. 6. A more even correction can be achieved when the low altitude DM corrects the low altitude *average* wavefront error of all LGS directions. This, however, results in a slight loss of Strehl ratio on-axis. For this paper, we chose the optimal correction of the field center.

The Strehl ratio for the wavefront variance $\sigma_{\text{fit}}^2 + \sigma_0^2$ of an MCAO system with 2 DMs is shown as a function of the angle between science object and

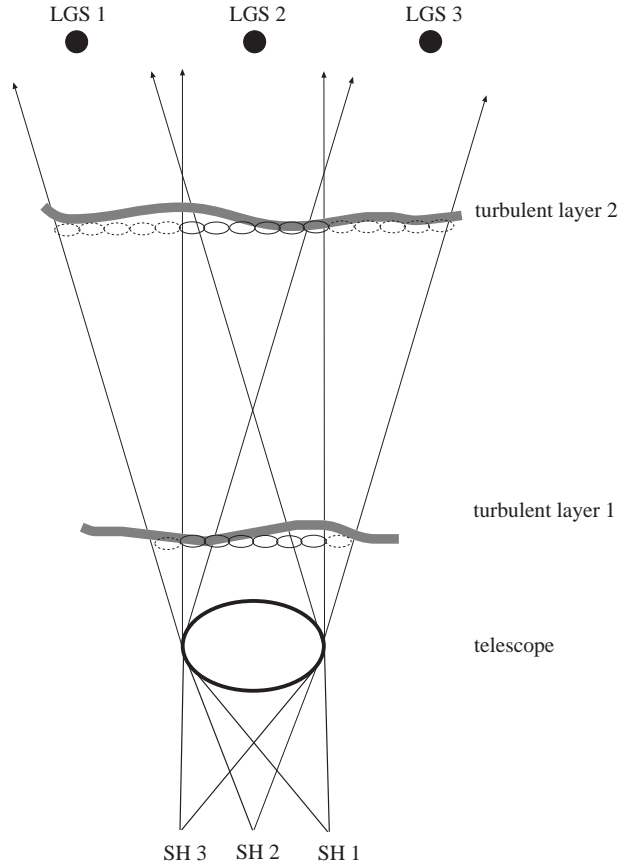


Figure 6. Side view of an MCAO geometry. Each circle in the turbulent layers indicates one Shack-Hartmann subaperture i.e. one actuator of the DM that is situated in the conjugate plane. Solid and dashed circles denote the correction for the central LGS and the other LGSs, respectively. At low altitudes, off-axis light cones mostly coincide with that of the (optimal corrected) central LGS, whereas at high altitudes, an independent correction of off-axis wavefronts is possible.

guide star for different numbers of corrected modes (Fig. 7) and different r_0 (Fig. 8). It is obvious that a high order correction at large angles θ results in a higher gain for the Strehl ratio in MCAO than in single DM AO systems. For our calculations we assumed that the absolute tip/tilt of the LGSs is known (see end of section 2). Due to the $(D/r_0)^{(5/3)}$ -law (see Eq. 5), both AO and MCAO systems heavily depend on good seeing to reach a high image quality.

Other possibilities of calculating the isoplanatic angle of MCAO systems are given by Tokovinin et al. (2000) and Wallner (1994). Their solutions, however, do not take the number of corrected modes into account.

A number of methods have been proposed to deal with the tip/tilt determination problem. Although it is possible to use only one natural guide

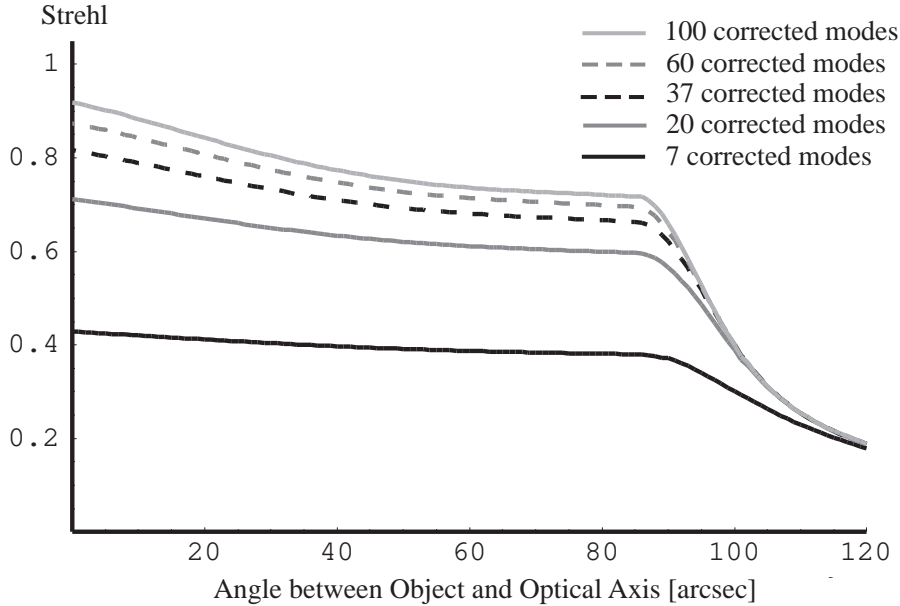


Figure 7. Strehl ratio for the wavefront variance $\sigma_{\text{fit}}^2 + \sigma_{\theta}^2$ of an MCAO (2 DMs) as a function of the number of corrected modes and the angle between science object and optical axis ($D = 3.5$ m, 37 corrected modes, Calar Alto C_n^2 -profile, K-Band, 7 LGS, $\alpha = 30^\circ$ (see Fig. 5)).

star (NGS) for absolute tip/tilt determination over the whole field of view (Johnston and Welsh, 1994), the wavefront reconstruction would not be as accurate as if the absolute tip/tilt was determined for each LGS. Since it is unlikely to find one NGS close to each LGS, the absolute tip/tilt of each LGS should be measured independently. Ragazzoni (1996) proposed to position and point auxiliary telescopes in such a way that one LGS and one NGS are in a line with one auxiliary telescope. Then the tip/tilt of each LGS can be determined by subtraction². Another possibility is the use of polychromatic LGSs (Foy et al., 1995), which excite two wavelengths in the sodium layer. The wavelength difference of the two colours leads to a differential tip/tilt caused by atmospheric dispersion, from which the absolute tip/tilt can be calculated. Unfortunately, for a sufficient excitation of the second colour, the laser output power has to be increased by about two orders of magnitude.

² Since one auxiliary telescope can measure tip *or* tilt, two auxiliary telescopes per LGS are required for absolute tip/tilt-determination.

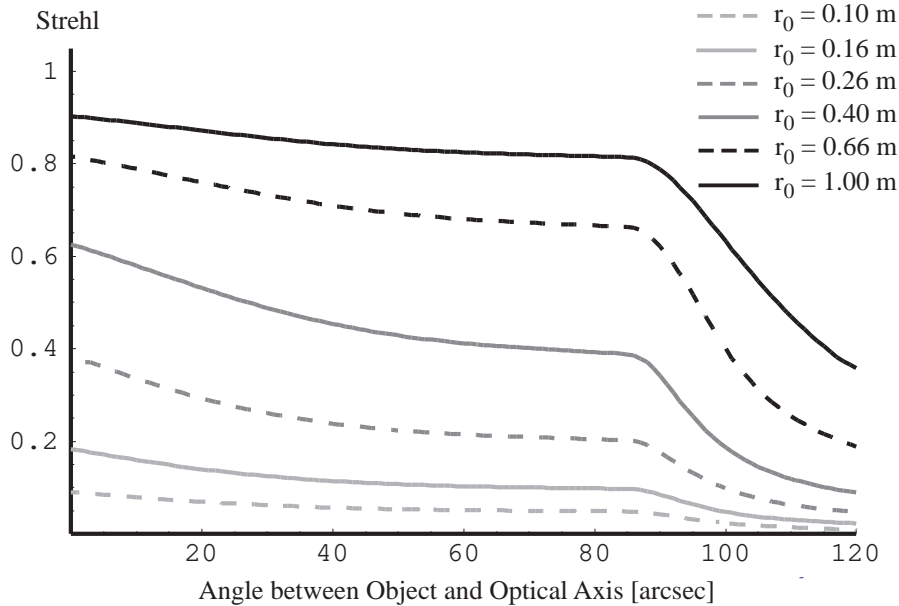


Figure 8. Strehl ratio for the wavefront variance $\sigma_{\text{fit}}^2 + \sigma_{\theta}^2$ of an MCAO (2 DMs) as a function of r_0 (scaled Calar Alto C_n^2 -profile) and the angle between science object and optical axis ($D = 3.5$ m, 37 corrected modes, 7 LGS, $\alpha = 30^\circ$ (see Fig. 5)).

3. Separating the wavefront distortion of high and low altitude turbulent layers

It has been shown in the previous section that 2-DM-MCAO systems already produce a wide and relatively evenly corrected field of view. In this section, we discuss methods to distinguish the wavefront aberrations of the corresponding two layers, a high and a low altitude layer.

One possibility is the use of tomographic methods, as proposed by Beckers (1988). Since a large number of LGSs is required, this method is quite demanding for night telescopes, but can be very useful for solar telescopes where no LGSs are needed. New aspects of zonal tomography can be found in Tallon and Foy (1990). The possibility of modal tomography has recently been shown by Ragazzoni (Ragazzoni et al., 1999)(Ragazzoni et al., 2000). Solar AO systems were discussed by Scharmer et al. (2000) and Rimmele et al. (1999).

In order to reduce the number of LGSs³ for measuring the individual wavefront distortion of two turbulent layers, the intensity information provided in each lenslet of a SH sensor can be used, as proposed by Ribak and Gershnik (1996). If the SH sensor is situated in the conjugate pupil plane,

³ However, the desired FOV should be completely covered by the LGS light cones.

the intensity variation at low light levels is dominated by photon noise. This situation can be improved by varying the position of the SH sensor as will be discussed in the following. For further SNR improvement and for reducing the error caused by the wavefront modes undetectable by scintillation, a second SH sensor can be used, effectively forming the SH-Curvature sensor.

Further aspects of wavefront separation and reconstruction can be found in (Roddier, 1988; Hickson and Burley, 1994; Ribak, 1996; Schwartz et al., 1994).

3.1. INTRODUCTION TO SCINTILLATION

Intensity fluctuations of star images (scintillation) are caused by the curvature of turbulent layers (second derivative of the phase, lensing effect, as shown in Fig. 9).

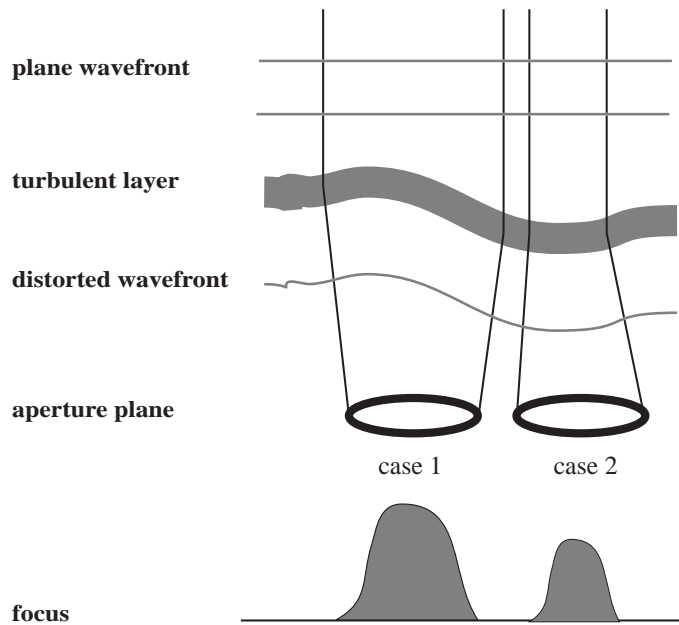


Figure 9. A turbulent layer focuses (case 1) or defocuses (case 2) the incoming light, resulting in a larger or smaller effective aperture in the focal plane.

Usually, astronomical observations are not affected by scintillation due to long integration times and large apertures. However, if intensity fluctuations of highly time-resolved measurements are not treated as noise, they can be used to provide information about the altitude distribution of turbulent layers. Good introductions to the theory of scintillation can be found in (Dravins et al., 1997a; Dravins et al., 1997b; Dravins et al., 1998; Elsässer and Siedentopf, 1959; Reiger, 1963).

The variance of the measured intensity σ_I^2 consists of the variance of the scintillation σ_S^2 and other noise sources (detector noise σ_D^2 and photon noise σ_P^2):

$$\sigma_I^2 = \sigma_S^2 + \sigma_D^2 + \sigma_P^2. \quad (10)$$

If the detector noise and the photon noise are known, the variance of the scintillation can be determined. According to Reiger (1963), the theoretical value of σ_S^2 is given by

$$\sigma_S^2 \propto D^{-7/3} (\cos \gamma)^{-3} \int z^2 C_n^2(z) dz, \quad (11)$$

D and γ denoting the telescope aperture and the zenith angle, respectively. Simulations with the program *Turbulence* (Berkefeld et al.,) have shown that the normalized variance of the intensity for a single layer at altitude z can be approximated by

$$\sigma_S^2 = D^{-7/3} \lambda^2 z^2 r_0^{-5/3} (\cos \gamma)^{-3}. \quad (12)$$

Because of $r_0 \propto \lambda^{6/5}$, the scintillation does not depend on the wavelength. For an extended turbulence profile one obtains

$$\sigma_S^2 = 16.7 \cdot D^{-7/3} (\cos \gamma)^{-3} \int z^2 C_n^2(z) dz. \quad (13)$$

Due to the factor z^2 the scintillation is mostly caused by high altitude turbulent layers. For $\sigma_S > 10\%$, e.g. for large zenith angles γ or for small telescope apertures D , the scintillation begins to become nonlinear, approaching a maximum value, and Eq. 13 is no longer valid (Dravins et al., 1997a; Protheroe, 1954).

3.2. WAVEFRONT SENSORS FOR SEPARATING THE CONTRIBUTIONS OF HIGH AND LOW ALTITUDE TURBULENT LAYERS

Since the wavefront gradient in each SH subaperture is the *sum* of the wavefront distortions of all turbulent layers, additional information is needed for distinguishing the influence of individual layers. By using the spatially resolved scintillation provided in each subaperture of the SH sensor, the distortion of one of the layers can be reconstructed. Together with the known sum of the aberrations, the wavefront distortion of the other layer can then also be determined (Fig. 10).

As in a conventional AO-setup, the SH sensor measures the tip/tilt in each subaperture, thus delivering the integrated wavefront error. Because the SH sensor is situated in the conjugate plane of one of the turbulent layers (subsequently named first layer), this layer has no effect on the intensity of the SH pattern. The - for the SH sensor - defocused other (subsequently named

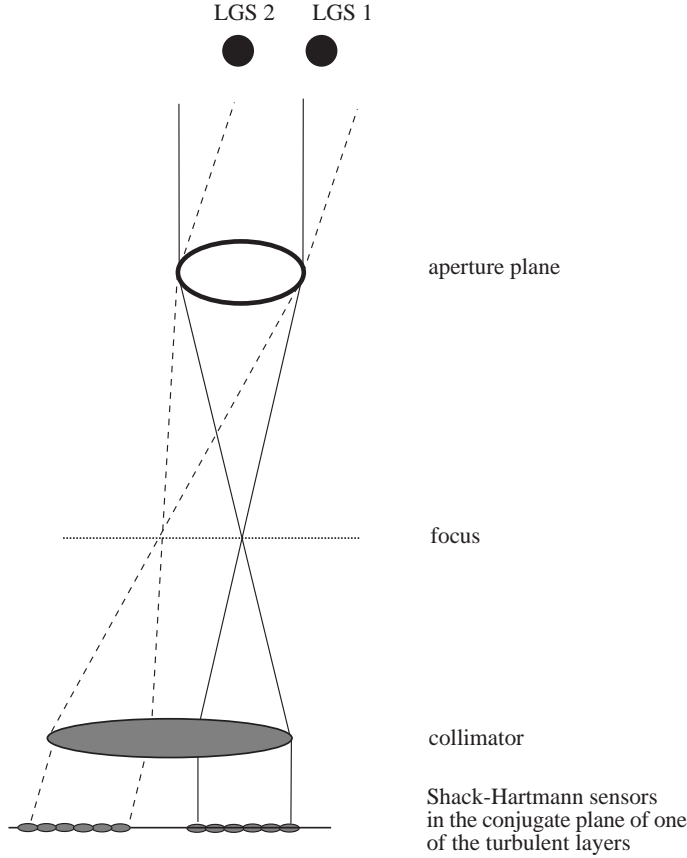


Figure 10. Setup of a wavefront sensor separating the wavefront distortions of two turbulent layers. For clarity, the light paths of only two guide stars have been plotted. One SH sensor per LGS is required.

second) layer leads to intensity fluctuations $I'_2(x'_2)$ in the subapertures from which the wavefront distortion ϕ of the second layer can be reconstructed (Ribak and Gershnik, 1996; Glindemann and Berkefeld, 1996):

$$I'_2(x'_2) = 1 - \frac{z'_2 - z'_1}{2k} \frac{\partial^2 \phi_1(x'_2)}{\partial x'^2_2}, \quad (14)$$

where indices denote the layers. z is the altitude coordinate, $k = 2\pi/\lambda$, and dashed variables indicate the conjugate planes. The radial wavefront tilt affects the intensity measurement at the edge of the aperture (Roddir, 1988). Although the edge radial tilts can be extracted directly from the SH tilt measurement and thus their contribution can easily be corrected, they must be known for each layer. They can be estimated by first determining the mean gradient m_i (averaged over all LGSs j) of each edge subaperture i . The m_i can be regarded as the edge gradients of the low altitude turbulence (which

are the same for all LGSs), whereas its deviation r_{ij} can be regarded as the high altitude gradients

$$r_{ij} = t_{ij} - m_i \quad \text{with} \quad m_i = \frac{\sum_{j=1}^n t_{ij}}{n}, \quad (15)$$

with t_{ij} being the measured gradients. It is obvious that this is only an approximation which will be more accurate with a higher number of LGS (and thus a larger corrected field of view). Once the wavefront distortion of one of the layers has been reconstructed, subtraction from the measured sum of the wavefront errors delivers the wavefront distortion of the other layer. The error made by averaging the radial gradients, as described by Eq. 15, is still unknown. This problem should therefore be addressed more closely in the future.

One can define the contribution of an individual layer i to the scintillation in a conjugate plane of altitude h by (see Eq. 13)

$$\sigma_{S,i}^2(h) = 16.7 \cdot D_{\text{sub}}^{-7/3} (\cos \gamma)^{-3} \int_{L_i} (z-h)^2 C_n^2(z) dz, \quad (16)$$

with D_{sub} the subaperture size of the SH sensor that is placed in the conjugate plane of altitude h .

The goal of the measurement is to determine the contribution of the more turbulent of the two layers. Thus, the SH sensor is placed in a conjugate plane where the scintillation of the more turbulent layer (in this case layer 2) is very large and the contribution of layer 1 is very small. Then, one can write the signal-to-noise ratio (SNR) as the normalized mean square error ($1/\text{SNR}^2$) of the intensity measurement as:

$$\frac{1}{\text{SNR}^2} = \frac{\frac{1}{N_r} + \frac{n \cdot R^2}{N_r^2} + \sigma_{S,1}^2(h)}{\sigma_{S,2}^2(h)}. \quad (17)$$

The numerator consists of the photon noise $1/N^{1/2}$, the read noise $R \cdot n^{1/2}$ (n is the number of pixels used for the intensity measurements, R denotes the readout noise per pixel), and the contribution of layer 1 that is treated as noise for the measurement of layer 2 that constitutes the signal in the denominator. The scintillation error due to the non discrete layering of the C_n^2 -profile is very small and need not be taken into account (Berkefeld, 1998).

Typically the measured scintillation is of the order of a few percent. This poses problems at low light levels where the scintillation competes with the shot noise. Although it is possible to measure the scintillation of the more turbulent layer (usually the ground layer) and thus get a smaller relative error, this does not lead to a better separation of the layers because the *absolute*

error of the wavefront reconstruction is also proportional to the turbulence strength. Therefore it does not matter whether the scintillation of the strong or the weak turbulence is measured. Instead, the mean square error can be reduced by moving the SH sensor further away from the conjugate plane of the first turbulent layer, as shown in Fig. 11.

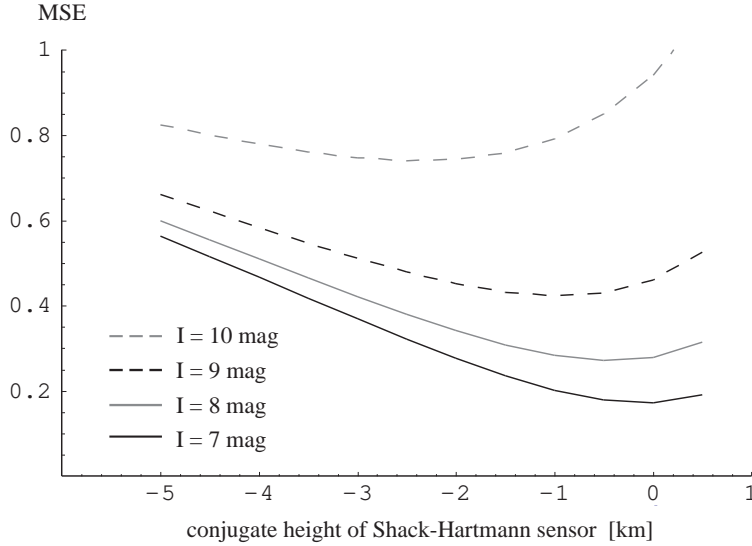


Figure 11. Normalized mean square error ($1/\text{SNR}^2$) of the scintillation measurements as a function of the conjugate altitude of the SH sensor for different LGS intensities. The sub-aperture size and the read noise have been assumed as $D_{\text{sub}} = 0.5$ m (35-40 corrected modes) $n = 16$ pixels and $R = 3e^-$, which are typical values for the AO system ALFA at the Calar Alto 3.5 m telescope. The integration time of the wavefront sensor was chosen to be optimal for each LGS brightness. In this figure, the scintillation caused by the high altitude turbulence is measured. Increasing LGS brightness leads to increasing optimal altitude of the SH sensor. In order to have an SNR better than 4 the mean square error has to be smaller than $1/16$.

Although this leads to an unwanted contribution to scintillation from the now defocused first layer, the SNR increases within certain limits due to the much higher scintillation signal from the second layer. However, in the case of a 589 nm LGS with a 10 mag G-star brightness equivalent, the maximum SNR is 1.15, which is not sufficient for wavefront separation.

3.3. THE SHACK-HARTMANN-CURVATURE SENSOR

For low light levels the amount of scintillation has to be increased by moving the SH sensor further away from the conjugate planes of the turbulent layers. Since the scintillation effects of two layers cannot be distinguished with one SH sensor, an additional SH sensor is necessary, forming the Shack-Hartmann-Curvature sensor. In order to refine the SHC setup presented by Glindemann and Berkefeld (1996) we propose to position the individual SH

sensors in such a way that a mean intensity fluctuation of 10% (the non-linearity limit of scintillation) is achieved in each SH sensor. This is the case at the conjugate planes of a very large positive altitude and a large negative altitude, leading to an excess of illumination in one plane and to a lack of illumination in the other, similar to the Curvature Sensor (Roddi, 1988). For the Calar Alto C_n^2 -profile this results in altitudes of approx. 16 km and -12 km.

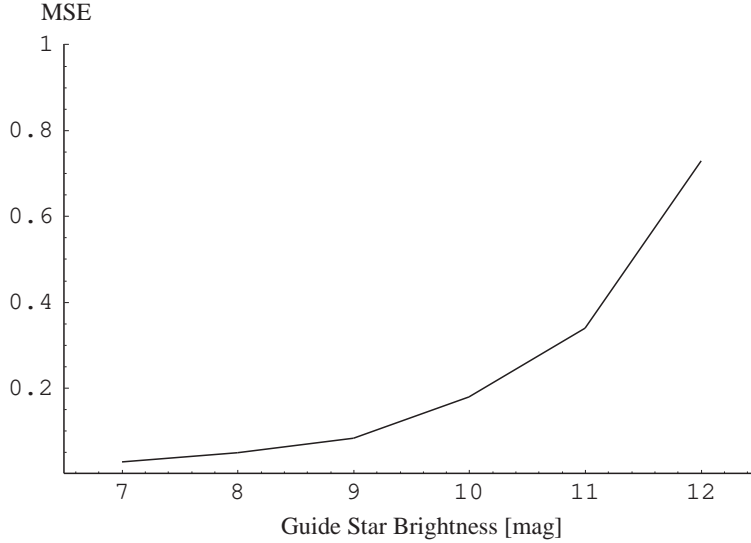


Figure 12. Normalized mean square error of the intensity measurements performed by a SHC sensor as a function of the guide star brightness. The conjugate altitudes of the SH sensors have been assumed as 16 km and -12 km, the other parameters are the same as in fig 11.

The scintillation variance $\sigma_{S,SHC}^2(h_1, h_2)$ of a SHC sensor can be expressed as the sum of two SH sensor signals each of which receives contributions of high and low altitude turbulence. For turbulence separation, the signal of each SH sensor is the difference of high and low altitude turbulence scintillation:

$$\sigma_{S,SHC}^2(h_1, h_2) = 16.7 \cdot D_{\text{sub}}^{-7/3} (\cos \gamma)^{-3} \times \quad (18)$$

$$\left(\int_{L_1} ((z-h_1)^2 + (z-h_2)^2) C_n^2(z) dz - \int_{L_2} ((z-h_1)^2 + (z-h_2)^2) C_n^2(z) dz \right)$$

Then, the mean square error for a SHC is:

$$1/\text{SNR}^2 = \frac{\frac{1}{N_\gamma} + \frac{nR^2}{N_\gamma^2}}{\sigma_{S,SHC}^2(h_1, h_2)} \quad (19)$$

An LGS brightness of 8 mag leads to an SNR of 4 which should be sufficient for most applications (see Fig. 12). Therefore observations in the NIR and

a typical LGS brightness of 10 mag require one SHC sensor per LGS. Observations in the visible require much more powerful LGSs in order to sense and correct a higher number of modes. Then, a single SH per LGS can be used. In any case, the C_n^2 -profile and the zenith angle should be monitored continuously in order to adjust the SH sensors and the DMs accordingly.

There is another aspect that makes the use of a SHC sensor more desirable than a SH sensor: Since the scintillation signals of the wavefront modes are not linearly independent, it is not possible to measure the wavefront modes of zero Laplacian with a SH sensor directly. Although it is possible to estimate these modes by averaging the radial wavefront tilts as described in section 3.2, the remaining error should be reduced further by using the intensity measurements for applying a priori (statistical) knowledge. Since a SHC sensor provides two and a SH sensor only one measurements per subaperture, the application of a priori knowledge will work better with a SHC sensor. However, for deriving a stable algorithm that operates in real-time, more detailed work has to be done in the field of wavefront reconstruction by intensity measurements.

4. Conclusion

By using MCAO, it is possible to overcome the most severe disadvantage of AO, the very small corrected FOV. We have shown how the geometry of MCAO systems affects the angular anisoplanatism and thus the size of the corrected FOV. A setup with seven LGSs for wavefront sensing leads to a wide and relatively evenly corrected field. In the case of the Calar Alto 3.5 m telescope, this setup would lead to a FOV of about three arcminutes. Eq. 5 plays an important role in calculating the wavefront error caused by angular anisoplanatism. By its minimization one obtains the optimal position of the DMs (according to the C_n^2 -profile). Since the remaining anisoplanatism inside the field is rather small, a wavefront correction with two DMs seems to be a good compromise between anisoplanatism, cost and system complexity. The separation of the wavefront errors of the two layers can be accomplished in various ways: For solar telescopes, tomographic methods, as proposed by Beckers, seem to be the most accurate and easy to implement way. For night telescopes, the separation can be done by using the intensity information provided by each lenslet of the SH sensor or SHC sensor. The SHC sensor should be preferred because it allows a fainter limiting magnitude and can reduce the separation error caused by the wavefront modes with zero Laplace operator.

The high costs for the LGS setup and the absolute tip/tilt determination will prevent MCAO systems from being used at existing 3.5 m-class-telescopes, at least as long as other improvements of conventional AO systems are possi-

ble. At 8+ m-class-telescopes however, focal anisoplanatism will require the use of multiple laser guide stars. Furthermore, the cost of MCAO systems compared to those of the telescope will decrease, so that MCAO will become a common feature at large telescopes.

Appendix

A. Calar Alto C_n^2 -profile

Fig. 13 shows a slightly simplified C_n^2 -profile measured by Klückers et al. (1998) at the Calar Alto Observatory, Spain. The upper turbulent layer at an altitude of 7 km delivers the main contribution to the angular anisoplanatism, the lower turbulent layer determines most of r_0 . For a 2-DM-MCAO, the optimal altitudes for the DMs are 400 m and 6900 m. It should be noted, that the turbulence profile can change rather quickly. Klückers reported a change of the upper turbulent layer strength by a factor of two in only a few minutes. Therefore, frequent C_n^2 -measurements should be made to adjust the optimum altitude of the DMs.

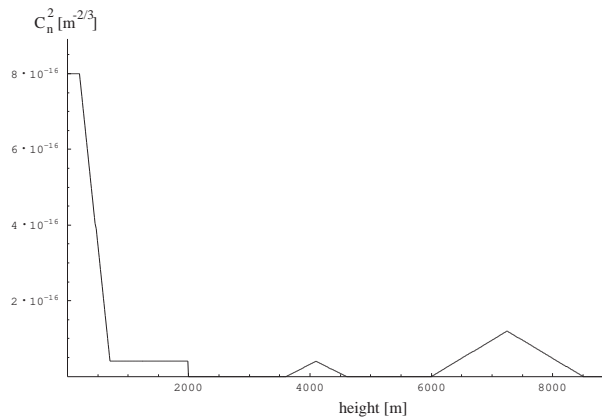


Figure 13. C_n^2 -profile at the Calar Alto Observatory (Klueckers et al., 1998), $r_0 = 66$ cm in K-band)

References

- Beckers, J.: 1988, 'ESO-Symposium on Large Telescopes and Their Instrumentation'. *ESO-Proceedings* p. 693.
- Berkefeld, T.: 1998, *Untersuchungen zur Messung und Korrektur einzelner Schichten der Erdatmosphäre*. Dissertation Universität Heidelberg.
- Berkefeld, T., A. Glindemann, and R. Weiss, 'in preparation'.

- Chassat, F.: 1989, 'Calcul du domaine d'isoplanétisme d'un système d'optique adaptative fonctionnant à travers la turbulence atmosphérique'. *J. Optics, Paris* **20**, 13.
- Dravins, D., L. Lindegren, E. Mezey, and A. Young: 1997a, 'Atmospheric Intensity Scintillation of Stars I. Statistical Distributions and Temporal Properties'. *Publ. Astron. Soc. Pac.* **109**, 173.
- Dravins, D., L. Lindegren, E. Mezey, and A. Young: 1997b, 'Atmospheric Intensity Scintillation of Stars II. Dependence on Optical Wavelengths'. *Publ. Astron. Soc. Pac.* **109**, 725.
- Dravins, D., L. Lindegren, E. Mezey, and A. Young: 1998, 'Atmospheric Intensity Scintillation of Stars III. Effects for Different Telescope Apertures'. *Publ. Astron. Soc. Pac.* **110**, 610.
- Elsässer, H. and H. Siedentopf: 1959, 'Zur Theorie der astronomischen Szintillation. I'. *Zeitschrift für Astrophysik* **48**, 213.
- Foy, R., A. Migus, F. Biraben, G. Grynberg, P. McCullough, and M. Tallon: 1995, 'The polychromatic artificial sodium star: A new concept for correcting the atmospheric tilt'. *Astronomy & Astrophysics supplement series* **111**, 569.
- Glindemann, A. and T. Berkefeld: 1996, 'A new method for separating atmospheric layers using a shack-hartmann curvature sensor'. In: *Adaptive Optics*, Vol. 13. OSA Technical Digest Series, p. 153.
- Hickson, P. and G. Burley: 1994, 'Single-image wavefront curvature sensing'. *SPIE* **2201**, 549.
- Johnston, D. and B. Welsh: 1994, 'Analysis of multiconjugate adaptive optics'. *J. Opt. Soc. Am.* **11**, 394.
- Klückers, V., N. Wooder, T. Nichols, M. Adcock, I. Munro, and J. Dainty: 1998, 'Profiling of atmospheric turbulence strength and velocity using a generalised SCIDAR technique'. *A & A Supplement Series* **130**, 141.
- Noll, R.: 1976, 'Zernike polynomials and atmospheric turbulence'. *J. Opt. Soc. Am.* **66**, 211.
- Protheroe, W.: 1954, 'Preliminary Report on Stellar Scintillation'. *Ohio State University* **4**.
- Ragazzoni, R.: 1996, 'Absolute tip-tilt determination with laser beacons'. *Astronomy & Astrophysics* **305**, L13.
- Ragazzoni, R., E. Marchetti, and F. Rigaut: 1999, 'Modal tomography for adaptive optics'. *Astronomy and Astrophysics* **342**, L53.
- Ragazzoni, R., E. Marchetti, and G. Valente: 2000, 'Adaptive-optics corrections available for the whole sky'. *Nature* **403**, 54.
- Reiger, S.: 1963, 'Starlight Scintillation and Atmospheric Turbulence'. *AJ* **68**, 395.
- Ribak, E.: 1996, 'Stellar Scintillations as a remote atmospheric wave-front sensor'. *Opt. Letters* **21**, 435.
- Ribak, E. and E. Gershnik: 1996, 'Stellar scintillation as a remote atmospheric wave-front sensor'. *Optics Letters* **21**, 6, 435.
- Rimmele, T., R. Radick, R. Dunn, and K. Richards: 1999, 'First Images from NSO's Solar Adaptive Optics System on the Internet'. *NOAO Newsletter* **57**, 31.
- Roddier, F.: 1988, 'Curvature sensing and compensation: a new concept in adaptive optics'. *Applied Optics* **27**, 7, 1223.
- Sasiela, R. and J. Shelton: 1993, 'Transverse spectral filtering and Mellin transform techniques applied to the effect of outer scale on tip/tilt anisoplanatism'. *J. Opt. Soc. Am.* **A10**, 646.
- Scharmer, G., M. Shand, M. Loefdahl, P. Dettori, and W. Wei: 2000, 'A Workstation Based Solar Adaptive Optics System'. *Proc SPIE* **4007**, 105.
- Schwartz, C., G. Baum, and E. Ribak: 1994, 'Turbulence-degraded wave fronts as fractal surfaces'. *J. Opt. Soc. Am. A* **11**, 1, 444.
- Tallon, M. and R. Foy: 1990, 'Adaptive telescope with laser probe: isoplanatism and cone effect'. *Astronomy and Astrophysics* **235**, 549.

- Tokovinin, A., M. L. Louarn, and M. Sarazin: 2000, 'Isoplanatic angle in a multi-conjugate adaptive optics system'.
- Tyson, R.: 1991, *Principles of Adaptive Optics*. Academic Press.
- Valley, G. and S. Wandzura: 1979, 'Spatial correlation of phase-expansion coefficients for propagation through atmospheric turbulence'. *J. Opt. Soc. Am.* **69**,5, 712.
- Wallner, E.: 1994, 'Optimizing the locations of multiconjugate wavefront correctors'. *Proc. SPIE* **2201**, 110.